Insight into the effect of phosphorus poisoning of Cu/zeolites with different framework towards NH<inf>3</inf>-SCR

N.B. When citing this work, cite the original published paper.

(article starts on next page)

Insight into the effect of phosphorus poisoning of Cu/zeolites with different framework towards NH₃-SCR

Aiyong Wang [a,b,*], Maria Elena Azzoni [c], Joonsoo Han [a], Kunpeng Xie [d], Louise Olsson [a,*]

[a] *Chemical Engineering and Competence Centre for Catalysis, Chalmers University of Technology, Gothenburg, SE 412 96 Gothenburg, Sweden*
[b] *International Joint Laboratory of Catalytic Chemistry, Department of Chemistry, Research Center of Nano Science and Technology, College of Sciences, Shanghai University, Shanghai 200444, China*
[c] *Politecnico di Milano, Dipartimento di Energia, Via La Masa, 34, 20156 Milano, Italy*
[d] *Volvo Group Trucks Technology, SE 405 08 Gothenburg, Sweden*

ARTICLE INFO

ABSTRACT

Cu/zeolites were prepared to elucidate the effect of phosphorus poisoning on different zeolite framework structures for NH₃-SCR. The results show that there are significant differences in phosphorus poisoning depending on the zeolite framework structure. The PO_3^-/PO_4^{3-} species gradually decreased along with an increase in P_2O_5 in the following order: Cu/SSZ-13, Cu/ZSM-5, and Cu/BEA. One possible reason could be the increased pore size of these zeolites, which results in less steric hindrance for larger P_2O_5 species. P_2O_5 is suggested to enhance the redox ability of Cu ions, which results in an increase in low-temperature activity in NH₃-SCR, whereas Cu ions were significantly poisoned by PO_3^-/PO_4^{3-}, resulting in low-temperature deactivation. Furthermore, the effect of phosphorus poisoning on the structure of Cu/ZSM-5 was found to be much greater than that of Cu/BEA and Cu/SSZ-13, possibly due to phosphorus attacked the surface defects of the zeolite, causing local expansion and cracking.

1. Introduction

Catalysts for emission control have attracted great attention due to the huge number of vehicles in the world [1,2]. The elimination of nitrogen oxides (NOₓ, where 90 % or more is NO), has become particularly important [3–5], and countries around the world have adopted strict legislations to limit NOₓ emissions.

Selective catalytic reduction is one of the most studied processes that can effectively eliminate NOₓ. Some of these processes have been industrialized, such as ammonia selective catalytic reduction, abbreviated as NH₃-SCR [6–12]. The selective reduction of NOₓ with the help of NH₃ has been widely used to eliminate NOₓ from the exhaust of engines [3,13], nitric acid plants [14], and power plants [15]. At present, a variety of catalytic systems are being extensively studied, among which V₂O₅-WO₃/TiO₂ is the most representative for stationary sources [16], and Cu/zeolites are used for mobile sources [4,5].

Up to now, copper ion-exchanged zeolites, e.g., Cu/CHA, have been the commercial NH₃-SCR material used for large-scale applications in diesel-powered vehicles, owing to the remarkable catalytic activity and long-term thermal stability [4,17]. Though Cu/zeolite catalysts show excellent performance, different substances (e.g., sulphur and phosphorus) in emissions may result in reversible or irreversible deactivation of Cu/zeolite catalysts [11,18]. The poisoning of phosphorus is generally considered irreversible through physical (i.e., pore blocking, surface masking, etc.) and chemical (i.e., interacting with active sites and the supports) mechanisms [18,19]. The volatile engine oils (e.g. lubricant ZDDP, zinc diakyl dithio phosphates) are typical sources of phosphorus in engine exhaust. For example, the American Petroleum Institute (API) regulations for phosphorus content in lubricants include 1200 ppm phosphorus for SH grade lubricants and less than 800 ppm phosphorus for SN grade lubricants, and this specification is also applied in many other markets, such as China. Our earlier studies [20–22] explored the effect of phosphorus on a copper-exchanged chabazite catalyst in SCR reactions and also compared the hydrothermal stability of fresh and P-poisoned samples. The properties of phosphorus and zeolite interactions were extensively studied to examine the behaviors of the catalysts towards different aspects, e.g., hydrothermal stability, acid sites, and catalytic performance. It was found that phosphorus can act as a

promoter on Cu/zeolite catalysts, where phosphorous can increase high-temperature selectivity/conversion owing to the inhibition of non-selective ammonia oxidation caused by the reaction of phosphorus and unexchanged copper oxide. However, phosphorous can also have negative effects, such as in the decline in low-temperature catalytic activity and high-temperature hydrothermal stability. The effect of phosphorus poisoning on two Cu ions, i.e., ZCuOH and Z2Cu, was also elucidated [21], and it was found that the poisoning of Z2Cu involved P_2O_5, but that PO_3^-/PO_4^{3-} was responsible for ZCuOH poisoning. As a promoter, one recent study [23] found that the proper addition of phosphate ions can prevent the destruction of the zeolite framework caused by harsh aging. This results in preserving the ion-exchanged copper ions and the remarkable NH_3-SCR activity of Cu/SSZ-13. Those authors have suggested that a small amount of phosphorus (approximately 1–2 wt%) in the exhaust gas may be beneficial for the hydrothermal stability of Cu/SSZ-13 with a low Si/Al ratio. In addition, low-phosphorus content has been suggested to enhance the catalytic activity of the SCR reaction [18]. Moreover, the addition of phosphorous was found to have only a minor impact on the SCR performance of Cu/FER catalysts. However, it was found that the poisoning effect of phosphorus was significant for the catalytic deactivation when co-addition with sodium was done [19].

As we know that CHA is a small-pore zeolite with an 8-membered ring, while MFI and BEA have a 10-membered ring and 12-membered ring, respectively. In addition, Cu/CHA is the current commercial SCR catalyst, and Cu/MFI or Cu/BEA is widely studied materials for SCR reaction. Therefore, these three materials are representative for studying the relationship between zeolite structure and phosphorus poisoning. However, according to our knowledge, a comparison of using CHA, MFI, and BEA framework on the mechanisms of the phosphorus poisoning of Cu/zeolites has not been studied, which is the objective of the current work. This study has provided a thorough investigation of phosphorus and zeolite interaction. We synthesized Cu/CHA, Cu/MFI, and Cu/BEA catalysts with analogous chemical components and studied them in detail using multiple techniques including ICP, XRD, BET, XPS, NH_3-TPD, H_2-TPR, NO-NH_3-TPR and NO_2-TPD.

2. Experimental methods

2.1. Catalyst synthesis

Three types of zeolites in H form were used as blank catalysts for copper ion-exchanged catalysts. H/SSZ-13 zeolite (CHA) with a Si to Al mole ratio of ~ 10 was synthesized following the detailed procedures described elsewhere [24]. Beta zeolite (BEA, CP814E from Zeolyst) and ZSM-5 zeolite (MFI, CBV2314 from Zeolyst) with Si to Al mole ratios of around 10 were used, and the SAR ratios were measured with ICP. The BEA and MFI zeolites (NH_4 forms) were transformed to H form by calcination at 550 °C for 4 h in static air in a furnace (5 °C /min).

Three Cu-loaded catalysts with the aforementioned zeolite supports were prepared with the wetness impregnation method with $Cu(NO_3)_2$ solution as the Cu precursor [25]. First, a calculated amount of Cu precursor was added to ethanol with magnetic stirring for 10 min. H form material (i.e., CHA, MFI, and BEA) was gently added to the Cu $(NO_3)_2$ solution, and then the mixing container was covered with foil and continuously stirred until the slurry became homogenously blue. After that, the obtained product was placed in a fume hood at room temperature overnight. The dried powder was well ground and calcined in static air at 600 °C for 8 h and thereafter at 750 °C for 2 h (2 °C/min).

Phosphorus poisoning of the Cu/zeolite catalysts was carried out using the incipient wetness impregnation (IWI) method with a diluted $(NH_4)_2HPO_4$ solution following the detailed procedures described elsewhere [26].We previously systematically studied three different methods of phosphorus poisoning [20,22,26,27] that included (1) the IWI method with $(NH_4)_2HPO_4$; (2) vapor-phase phosphorus exposure with aqueous H_3PO_4 solution; (3) phosphorus poisoning with biodiesel

exhausts using a diesel burner aging rig. It was found that the phosphorus species formed on the catalyst using the three phosphorus poisoning methods had considerable similarities. It is also found that catalyst performance was similarly affected when the phosphorus content was similar. Therefore, the IWI method was applied to better control the phosphorus poisoning amount in the three zeolites in this study. Note that the P-poisoned catalysts were calcined at 550 °C for 4 h in static air in a furnace. The theoretical value of P to Cu molar ratio ~ 1.0 was used for all the catalysts. According to our previous study [22], when the phosphorus content was too low (i.e. P/Cu less than 0.5), its effect on the catalytic performance was not obvious, while when the phosphorus content was too high it is a risk that the effect of the zeolite structure will be masked. We therefore choose a moderate phosphorus content, i.e. P/Cu ratio ~ 1. Three Cu/zeolite catalysts with different frameworks were denoted Cu/SSZ-13_F, Cu/ZSM-5_F, and Cu/BEA_F, and the P-poisoned catalysts were denoted Cu/SSZ-13_P, Cu/ZSM-5_P, and Cu/BEA_P.

The powder of fresh and P-poisoned Cu/zeolite catalysts was loaded onto monoliths with a length of 20 mm and a diameter of 22 mm and a cell density of 400 cpsi. Details are described in our earlier work [28]. To improve the adhesion of the powder onto the monoliths during wash-coating, Disperal *P*2 from Sasol was co-added as a binder. The mass ratio between catalyst powder and binder was around 95 to 5. The entire loading amount was about 700 mg. The obtained monolithic catalysts were calcined at 500 °C for 2 h in static air in a furnace.

2.2. Flow reactor measurements

All the activity experiments were carried out on monolithic catalysts in a horizontal quartz tube. Details are described elsewhere [28]. Concentrations of reactants and products (e.g., NH_3, NO, H_2O, etc.) were recorded in real time using the MultiGas FTIR spectroscopy gas analyzer (MKS 2030 model). A flow rate of 2800 ml/min with a GHSV of 22,100 h^{-1} was applied in all the experiments. Before reactions, the as-prepared monolithic catalysts were degreened at 500 °C for 2 h using 400 ppm NO, 400 ppm NH_3, 5 % H_2O, and 8 % O_2 in Ar. Also note that the catalysts were pre-treated using 8 % O_2 in Ar at 550 °C for 30 min between standard NH_3-SCR and NH_3 oxidation.

Standard NH_3-SCR tests were carried out using 400 ppm NH_3, 400 ppm NO, 5 % H_2O, and 8 % O_2 in Ar with a total flow rate of 2800 ml/min. The monolithic catalysts were heated to 550 °C and maintained at that temperature for 30 min in the reaction gases, and then the temperature was stepwise reduced to 100 °C (20 °C/min) and maintained at each targeted temperature for 30 min.

The NH_3 oxidation tests were carried out using 400 ppm NH_3, 5 % H_2O, and 8 % O_2 in Ar with a total flow rate of 2800 ml/min. First, the monolithic catalysts were exposed to the gas mixture at 550 °C for 30 min, and then the temperature was gradually decreased to 300 °C (20 °C/min), and at each step the temperature was maintained for 30 min.

2.3. Catalyst characterization

The results of the inductively coupled plasma (ICP) analysis of the Cu, P, Si, and Al content of the catalysts were provided by ALS Scandinavia AB.

Specific surface areas (BET method) and pore volumes (*t*-plot method) were acquired with a Tristar 3000 instrument (Micromeritics) through the nitrogen adsorption and desorption isotherms. The samples were placed in liquid nitrogen, i.e., 77 K. Prior to the tests, the catalyst powder was degassed at 250 °C overnight in a continuous N_2 flow.

X-ray diffraction (XRD) was conducted on a BrukerAXS-D8 advance instrument equipped with an Ni-filtered copper K-alpha radiation with an X-ray wavelength of 1.5418 Å (40 kV, 40 mA). Spectra were recorded at 5-40° (2 theta) with 0.02° steps.

X-ray photoelectron spectroscopy (XPS) was obtained with a PHI

Versa Probe Microprobe using mono-chromatic Al Kα X-rays (hν = 1486.6 eV). The energy resolution (FWHM) was 0.646 eV. The instrument was calibrated through Au 4f7/2 = 83.96 eV, Ag 3d5/2 = 368.21 eV, and Cu 2p3/2 = 932.62 eV. During the analysis, the XPS spectra were calibrated using the C 1 s spectrum at 284.8 eV.

NH$_3$ temperature-programmed desorption (NH$_3$-TPD) was performed using monoliths in the NH$_3$-SCR setup to acquire the NH$_3$ adsorption/desorption of the weak/strong acid sites of the catalysts. The procedure was as follows: (1) pre-treat the catalyst at 550 °C using 8 % O$_2$ in Ar for 30 min; (2) cool sample to 100 °C, then turn off O$_2$, and maintain Ar flow for 10 min; (3) adsorb 400 ppm NH$_3$ in Ar at 100 °C for 1 h; (4) turn off NH$_3$ and maintain Ar flow for 20 min at 100 °C; and (5) ramp from 100 °C to 600 °C (20 °C/min).

H$_2$ temperature-programmed reduction (H$_2$-TPR) was carried out using a differential scanning calorimeter (DSC). The outgoing gas from the main line was introduced into the mass spectrometer (Hiden HPR-20 QUI MS) for H$_2$ detection. The experiment was performed from 25 to 800 °C at a ramp rate of 10 °C/min with 2000 ppm H$_2$ in Ar.

NO temperature-programmed reduction (NO-NH$_3$-TPR) was conducted to evaluate the redox capacity of copper species close to the condition of a real NH$_3$-SCR reaction. The procedure was as follows: (1) pre-treat the catalyst at 550 °C using 8 % O$_2$ in Ar for 30 min; (2) cool the sample to 50 °C, then turn off O$_2$, and maintain Ar flow for 10 min; (3) purge 400 ppm NO, 400 ppm NH$_3$ in Ar at 50 °C for 1 h; (4) maintain NO and NH$_3$ gases and ramp from 50 to 400 °C at a rate of 20 °C /min, and finally maintain the temperature at 400 °C for 10 min.

NO$_2$ temperature-programmed desorption (NO$_2$-TPD) was used to study the interaction between NO$_x$ and the surface copper sites. The NO$_2$-TPD procedure was conducted similar to the procedure for NH$_3$-TPD, except that 400 ppm NO$_2$ was added instead of 400 ppm NH$_3$. The maximum desorption temperature was set at 550 °C.

Note that some powder from each catalyst was degreened at 500 °C for 2 h using 400 ppm NO, 400 ppm NH$_3$, 5 % H$_2$O, and 8 % O$_2$ in Ar for BET, XRD, XPS, and H$_2$-TPR characterizations.

3. Results and discussion

3.1. Characterizations

The influence of phosphorus poisoning on three types of Cu/zeolites, i.e., Cu/SSZ-13, Cu/ZSM-5, and Cu/BEA, with comparable chemical compositions was extensively investigated. Table 1 presents the Cu and P contents, the Si to Al ratio, the Cu to Al ratio, and the P to Cu ratio of the fresh and P-poisoned samples. The Si/Al ratios of Cu/zeolites were approximately 8 ~ 10, and the corresponding Cu/Al ratios were controlled at 0.25 ~ 0.35 to ensure that the majority of copper was located at ion-exchanged sites. The P/Cu ratios were calculated and found to be ca 0.8 ~ 1.1 for all three P-poisoned samples.

Table 1 also shows the specific surface areas using the BET method and pore volumes using the *t*-plot method for fresh and P-poisoned Cu/zeolite catalysts. Small differences were found in Cu/SSZ-13 and Cu/BEA catalysts upon phosphorus poisoning, with a decline less than 5 % [21]. A moderate decrease in S$_{BET}$ and V$_{pore}$ was observed in Cu/ZSM-5, approximately 10–20 %. These results suggest that the structure of the Cu/ZSM-5 catalyst experienced a certain degree of damage after

phosphorus poisoning or possibly pore blocking, which was not found for the structures of CHA and BEA.

X-ray diffraction analysis was conducted to detect possible changes in zeolite structure after phosphorus poisoning [6]. The obtained XRD patterns for all samples (panel a) and enlarged peaks (panels b-d) are presented in Fig. 1. Only minor changes were detected for Cu/SSZ-13 (panel b) and Cu/BEA (panel d), which indicates that the framework structure of these materials was maintained mostly intact after phosphorus poisoning [18,23]. A comparison of the diffraction peaks for fresh and P-poisoned Cu/ZSM-5 samples (panel c) clearly shows a decrease in the crystallinity of this zeolite as a result of phosphorus poisoning, in line with the decrease in BET surface area and pore volumes. No CuO phase located at peaks of 35.55° and 38.70° was found in the XRD pattern of P-poisoned Cu/ZSM-5, despite obvious structural damage [29]. Kwak et al. [30] clearly observed CuO peaks caused by the destruction of the zeolite structure in different Cu ion-exchanged zeolites as a result of poisoning/hydrothermal aging. It is well known that phosphorus species (e.g., phosphate ions and phosphorus oxides) not only bonds to ion-exchanged Cu active sites, but these species can also possibly interact with Brønsted acid sites (likely with phosphate ions due to the basic nature) and surface hydroxyls/structural defects [22,26]. It is possible that the decrease in the crystallinity of the Cu/ZSM-5 sample was caused by the effect of phosphorus on acid sites instead of copper sites. In addition, the zeolite diffraction peaks shifted to lower angles in the P-poisoned Cu/ZSM-5 sample than in its fresh counterpart (panel c), which indicates that the lattice spacing of the zeolite structure expanded (approximately 0.005214 nm) in accordance with Bragg's equation ($d = \frac{n\lambda}{2sin\theta}$) [22]. This peak shift phenomenon was visible but minor in Cu/SSZ-13 (panel b), and it was undetected in Cu/BEA (panel d).

The distribution of phosphorus species among these P-poisoned samples was explored with the aid of XPS analysis. Fig. 2a shows the plots for the normalized XPS spectra of P 2p of Cu/SSZ-13_P, Cu/ZSM-5_P, and Cu/BEA_P samples. Three main types of phosphorus species are proposed based on the peak fitting. These species were identified as the oxide state, i.e., P$_2$O$_5$ centered at ca 135.6 eV, and anionic states, including PO$_3^-$ at ca 134.5 eV and PO$_4^{3-}$ at ca 133.4 eV. Similar species can be found in the literature [21]. The percentages of P$_2$O$_5$, PO$_3^-$, and PO$_4^{3-}$ species were obtained through area integration and are shown in Fig. 2b. The results clearly show that the type of zeolite framework significantly influences the types of P species formed on the Cu/zeolite. The Cu/SSZ-13 sample exhibited a large amount of PO$_3^-$ and PO$_4^{3-}$, which was less on the Cu/ZSM-5 sample and even less on the Cu/BEA sample. At the same time as PO$_3^-$ and PO$_4^{3-}$ species decreased, P$_2$O$_5$ species increased. One possible reason for this could be related to the increased pore size of the zeolite (CHA (~3.8 Å), MFI (~5.5 Å), to BEA (~6.6 Å)). The increased pore size could result in less steric hindrance for P$_2$O$_5$ species, which could explain the large amount of P$_2$O$_5$ found in the Cu/BEA sample. However, there could also be other possible reasons for the differences between these three zeolite samples, such as Brønsted acid strength, the distribution of Cu species (i.e., Z2Cu and ZCuOH).

More than 80 % of the phosphorus in the Cu/BEA sample did not chemically react with the catalyst but was simply in the physical state form (P$_2$O$_5$). P$_2$O$_5$ can form polycyclic dimers (P$_4$O$_{10}$) that then physically block the catalyst [31]. Note that although the Cu/BEA sample

Table 1
ICP analysis results, BET surface areas (S$_{BET}$), and pore volumes (V$_{pore}$) for all samples.

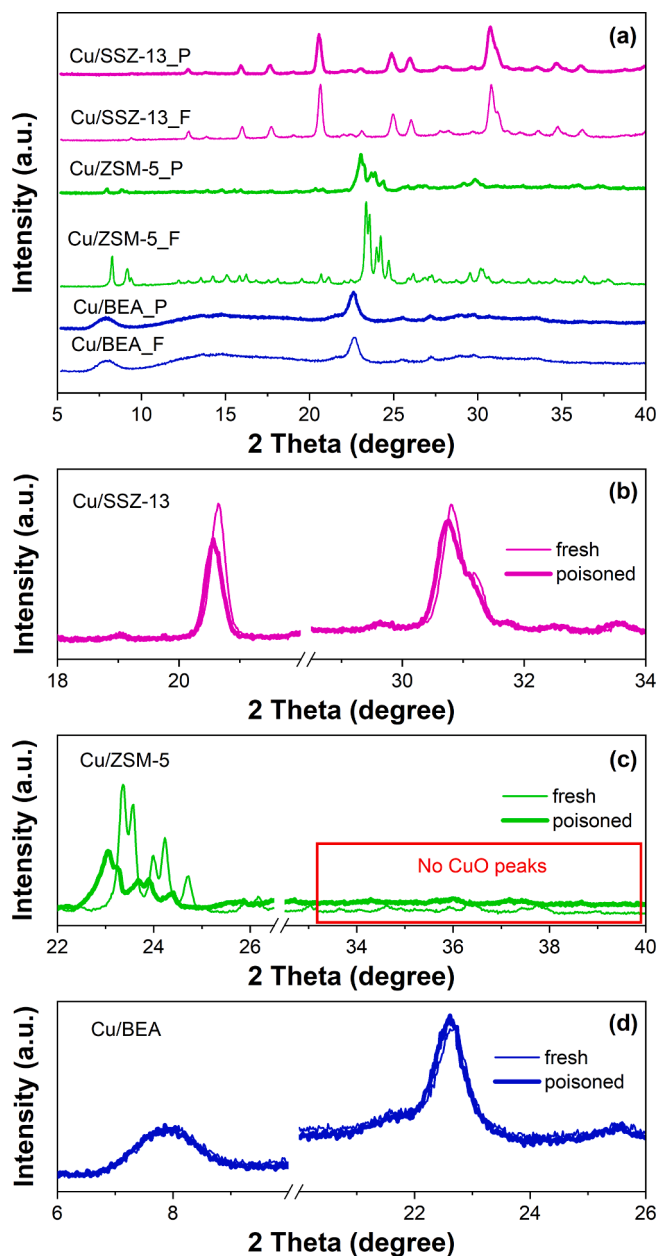| Sample	Cu (wt.%)	Si (wt.%)	Al (wt.%)	P (wt.%)	Si/Al ratio	Cu/Al ratio	P/Cu ratio	S$_{BET}$ (m^2/g)	V$_{pore}$ (cm^3/g)
Cu/SSZ-13_F	3.1	31.0	3.7	–	8.1	0.35	–	653	0.30
Cu/SSZ-13_P	2.9	30.0	3.6	1.25	8.0	0.34	0.88	639	0.29
Cu/ZSM-5_F	2.1	33.9	3.3	–	10.0	0.27	–	397	0.15
Cu/ZSM-5_P	2.0	34.1	3.2	0.93	10.2	0.26	0.97	344	0.12
Cu/BEA_F	1.8	36.3	3.2	–	10.8	0.24	–	566	0.17
Cu/BEA_P	1.8	34.9	3.3	0.94	10.1	0.23	1.06	562	0.17

Fig. 1. XRD patterns for: (a) fresh and P-poisoned Cu/BEA, Cu/ZSM-5 and Cu/SSZ-13 samples; (b) enlarged fresh and P-poisoned Cu/SSZ-13 samples; (c) enlarged fresh and P-poisoned Cu/ZSM-5 samples; (d) enlarged fresh and P-poisoned Cu/BEA samples.

contained a large amount of P_2O_5, the impact on the BET surface areas was negligible, as seen in Table 1. This can be attributed to the large aperture of BEA, ∼ 6.6 Å [31,32]. Also, it is possible that part of the P_2O_5 was on the surface of zeolite crystal and did not lead to a reduction in the BET areas.

Cu 2p XPS were also performed on the P-poisoned Cu/zeolites and the spectra are shown in **Fig. S1**. As can be seen in the figure, the peak positions of Cu 2p3/2 are at 933.1 eV and 935.9 eV for P-poisoned Cu/SSZ-13 samples, respectively, suggesting two different Cu(II) components. The peak at 933.1 eV was assigned to Z2Cu/ZCuOH and the peak at 935.9 eV was assigned to $Cu_3(PO_4)_2/Cu(PO_3)_2$ [33]. The peak positions of Cu2p3/2 were similar in the analysis of P-poisoned Cu/ZSM-5 sample (**Fig. S1**b), (933.6 eV and 936.7 eV), thus indicating the presence of Z2Cu/ZCuOH and $Cu_3(PO_4)_2/Cu(PO_3)_2$. However, it is clear that the amount of copper phosphate formed in the Cu/ZSM-5 sample is

considerably smaller than that in the Cu/SSZ-13 sample. Cu 2p XPS was also performed over the P-poisoned Cu/BEA sample shown in **Fig. S1**c, where the peak position of Cu 2p3/2 was mostly centered at 933.7 eV. It is known that the interaction between Cu active sites and NH_3 is a crucial step in the SCR reaction mechanism [34,35]. Therefore, these changes are critical to SCR performance, which will be discussed in Section 3.2 in combination with the flow reactor results.

The nature of acid sites before and after phosphorus poisoning were studied with NH_3-TPD analysis [36]. The complete NH_3 adsorption/desorption results are presented in **Fig. S2** for the fresh and P-poisoned Cu/zeolites. Enlarged curves of the NH_3 desorption regions are shown in Fig. 3a. A decline in NH_3 storage capacity was found for all P-poisoned catalysts in comparison to the corresponding fresh ones, which was reflected in the shorter NH_3 breakthrough time (**Fig. S2**) and weaker NH_3 desorption feature (Fig. 3a) [19,21].

To better understand the changes in NH_3 desorption for various zeolite frameworks upon phosphorus poisoning, the desorption areas were integrated. The obtained results are plotted in Fig. 3b. Note that these values were normalized to an NH_3 desorption amount from 700 mg washcoat. It is clear that the Cu/SSZ-13 sample had a significantly greater decrease in NH_3 storage capacity than the Cu/ZSM-5 and Cu/BEA samples after phosphorus poisoning. Cu/SSZ-13 showed the largest decline in NH_3 storage capacity (ca 25 %), although the total content of phosphorus was similar for these P-poisoned samples. This finding could be related to the XPS profiles (Fig. 2), where it was found that PO_3^-/PO_4^{3-} is the main species in Cu/SSZ-13, and P_2O_5 is dominant in Cu/BEA. Combining these two characterization results, it can be inferred that P_2O_5 has a smaller impact on the amount of adsorbed NH_3.

The subtracted curves (i.e., the NH_3-TPD curve for fresh samples (solid line) minus that for poisoned samples (dashed line)) are presented in Fig. 4a. Note that NH_3-TPD experiments were performed in the absence of H_2O to better observe the adsorption of NH_3 onto surface hydroxyls/structural defects. In line with the literature [20,37,38], the desorption curve of NH_3 from low- to high-temperature conditions was mainly composed of three parts: NH_3 desorbed from surface hydroxyls/structural defects, Cu ions, and Brønsted acid sites. The temperature of desorption of NH_3 from surface hydroxyls/structural defects was mainly between 150 and 200 °C, while the desorption temperatures from the Cu sites and the Brønsted acid site were in the region of 250 ∼ 350 °C and 400 ∼ 550 °C, respectively. Marberger et al. [39] have found that the desorption of NH_3 from Brønsted acid sites occurs at around 450 °C in the fresh Cu/SSZ-13 catalyst, which is consistent with this work. Fig. 3 (400 ∼ 550 °C) shows that the amount of NH_3 desorbed from Brønsted acid sites in the Cu/SSZ-13 sample was relatively small, which is due to that part of the Brønsted acid sites were replaced with Cu ions. Note that the desorption of NH_3 from surface hydroxyls/structural defects (150 ∼ 200 °C), i.e., surface hydroxyls and structural defects [18], on the Cu/ZSM-5 sample was much stronger than the desorption of the other two samples, as seen in Fig. 3a. It can be inferred that more surface hydroxyls/structural defects were present in the Cu/ZSM-5 sample. According to the N_2 adsorption–desorption isotherms, the external surface areas were 27 m^2/g (Cu/SSZ-13), 56 m^2/g (Cu/ZSM-5), and 201 m^2/g (Cu/BEA). It can be seen that Cu/ZSM-5 had a much larger external surface area than Cu/SSZ-13 but less than Cu/BEA. This could be explained that despite the large external specific surface area of Cu/BEA there were fewer defects on its grain integrity surface.

Peak deconvolution was used to evaluate the loss of desorbed NH_3 for different sites after phosphorus poisoning. The collected results from relative area integration are presented in Fig. 4b for comparison. Clearly, all three types of NH_3 desorption sites in these catalysts had experienced varying degrees of decline in NH_3 storage capacity after phosphorus poisoning. A significant difference in the distribution of the decline of NH_3 was found for different Cu/zeolites. It is worth noting that the dominant site for the decline in NH_3 storage capacity for the Cu/SSZ-13 sample was the Cu ions, accounting for approximately 69 %. The decrease in NH_3 storage capacity on Brønsted acid sites and surface
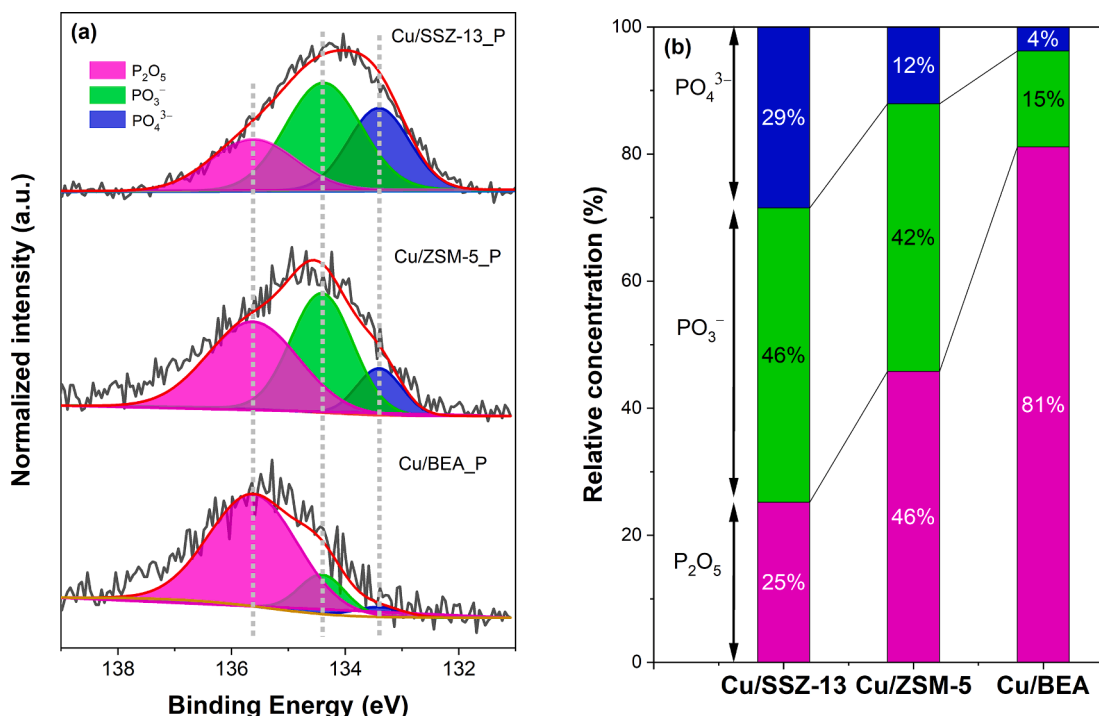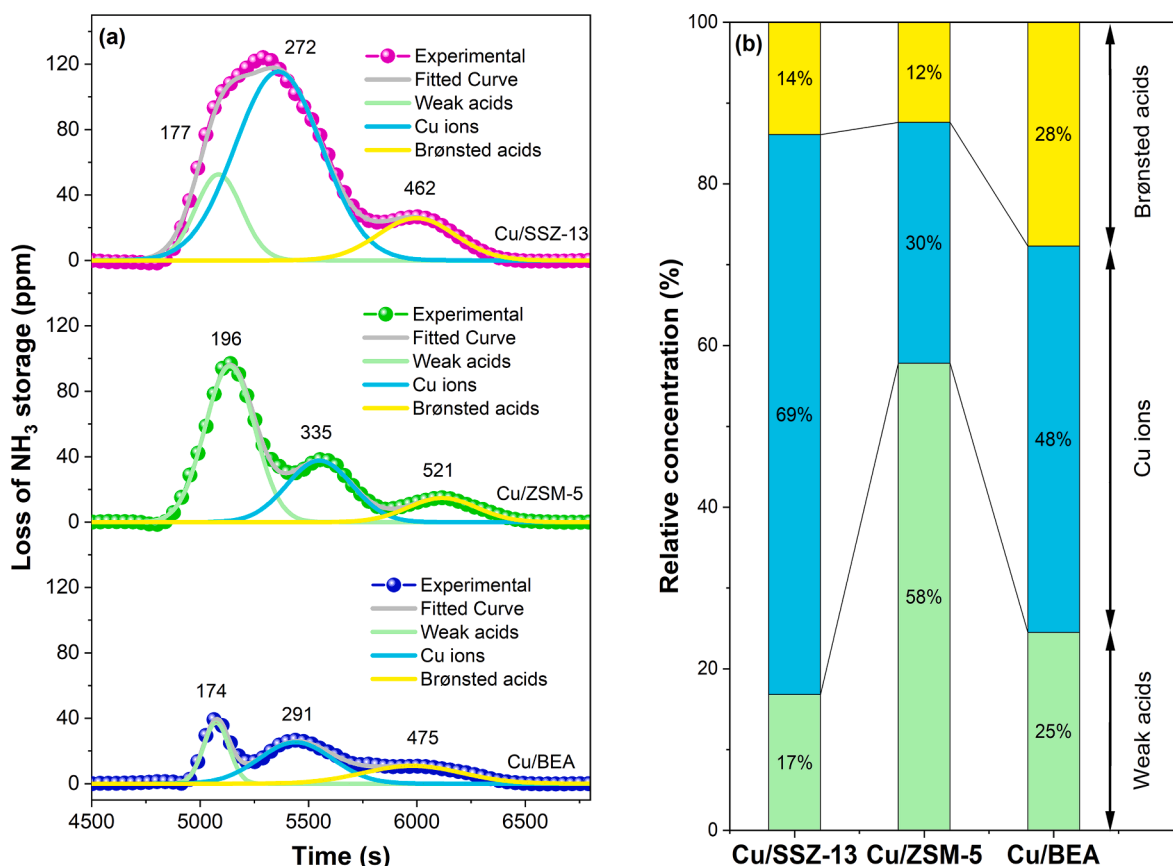
Fig. 4. (a) The subtracted curves (Fresh – P-poisoned) from NH$_3$-TPD for Cu/BEA, Cu/ZSM-5 and Cu/SSZ-13 samples; (b) The relative loss of NH$_3$ desorbed from the three sites affected by P-poisoning acquired by using the peak fitting of the results in (a).

Cu/ZSM-5, which can possibly explain why the ratio of H$_2$/Cu is low. In the same way, we propose that this is also the reason for the low H$_2$/Cu ratio for Cu/BEA. Also, note that the H$_2$ concentration used in this work was only 2000 ppm for the TPR experiments, which might result in less complete reduction of Cu^{2+}. Interestingly, the significant enhancement in H$_2$ consumption after phosphorus poisoning suggested that a portion of the copper ions poisoned by phosphorus would be directly reduced to Cu^0 in TPR tests. For the NO-NH$_3$-TPR discussed later in Fig. 6, the samples were pretreated at 550 °C using 8 % O$_2$ in Ar for 30 min, where Cu$^+$ could be re-oxidized to Cu^{2+}. A NO/Cu consumption ratio close to one was found, showing that all Cu sites are accessible. Note that the consumption of H$_2$ that was caused by the reduction of phosphorus species was excluded, according to our prior work; no H$_2$ consumption was found for the P-poisoned H/SSZ-13 sample using the H$_2$-TPR test [22] and the reduction temperature of copper phosphates was above 1000 °C [42], i.e. significantly above our examined temperature interval.

It is interesting to discover that the fresh samples showed smooth reduction features with increasing temperature, while the P-poisoned samples showed some sharp reduction peaks appeared. Note that the smooth reduction curves do not mean that only one reduction process occurred in the fresh catalysts. For example, one shoulder is apparent at 200 ~ 300 °C in the TPR curve of the fresh Cu/SSZ-13 sample, accompanied by a main peak at ~ 450 °C. This suggests that the different reduction peaks overlapped during the TPR. Similar results were also found for the other two Cu/zeolites.

The P-poisoned samples showed newly emerged peaks that are related to the phosphorus species that interacted with the Cu ions [21,22]. The sharp reduction peaks in the three poisoned samples were divided into two groups: the lower peak centered at 350 ~ 400 °C (denoted T1), and the higher one at 450 ~ 500 °C (denoted T2).

Considering the presence of P$_2$O$_5$ and PO$_3^-$/PO$_4^{3-}$ species, it was deduced that two different phosphorus-Cu complexes, e.g., P$_2$O$_5$-Cu ions and PO$_3^-$/PO$_4^{3-}$-Cu ions, were formed in these catalysts. The findings for P$_2$O$_5$ interacted with Z2Cu and PO$_3^-$/PO$_4^{3-}$ interacted with ZCuOH were shown in our previous work [40], where we synthesized a series of Cu/SSZ-13 with different Cu active sites distribution. The dominant Cu species residing in one sample was Z2Cu sites, whereas ZCuOH was the dominant species in another sample. Combined with different experiments, we found that the poisoning of Z2Cu involves two P atoms, i.e., P$_2$O$_5$, but only one P atom (PO$_3^-$), or fewer (PO$_4^{3-}$), is needed for ZCuOH poisoning. Note that only one dominant reduction peak appeared in Cu/SSZ-13 (only T2) and Cu/BEA (only T1), while both T1 and T2 appeared in Cu/ZSM-5 after phosphorus poisoning. PO$_3^-$/PO$_4^{3-}$ was the main phosphorus species in the Cu/SSZ-13 sample in XPS results (Fig. 2), and P$_2$O$_5$ was the main species in the Cu/BEA sample. Since no H$_2$ consumption was found for the P-poisoned H/SSZ-13 sample using the H$_2$-TPR test reported in our previous work [22], so we assume that PO$_3^-$/PO$_4^{3-}$ species were not reducible in the temperature region of this study. Consequently, it is reasonable to infer that T1 is assigned to the reduction of Cu ions interacting with P$_2$O$_5$, while T2 is from the Cu ions that interacted with PO$_3^-$/PO$_4^{3-}$. It is worth mentioning that our prior work [21] showed that T2 was found to shift to a lower temperature as the amount of Cu ions-P$_2$O$_5$ increased in the Cu/SSZ-13 sample, but T1 was not observed. Therefore, the framework of zeolite probably also plays an important role in distinguishing T1 and T2. A detailed examination revealed that P$_2$O$_5$ seemed to shift the reduction temperature of Cu ions to low temperatures in the Cu/ZSM-5 and Cu/BEA samples, i.e., P$_2$O$_5$ enhanced the redox ability of Cu ions. This will be further discussed in conjunction with data in Section 3.2.

Inspired by the pioneering studies by Hammershoi et al. [43] and Villamaina et al. [44], the NO-NH$_3$-TPR method with a NO and NH$_3$
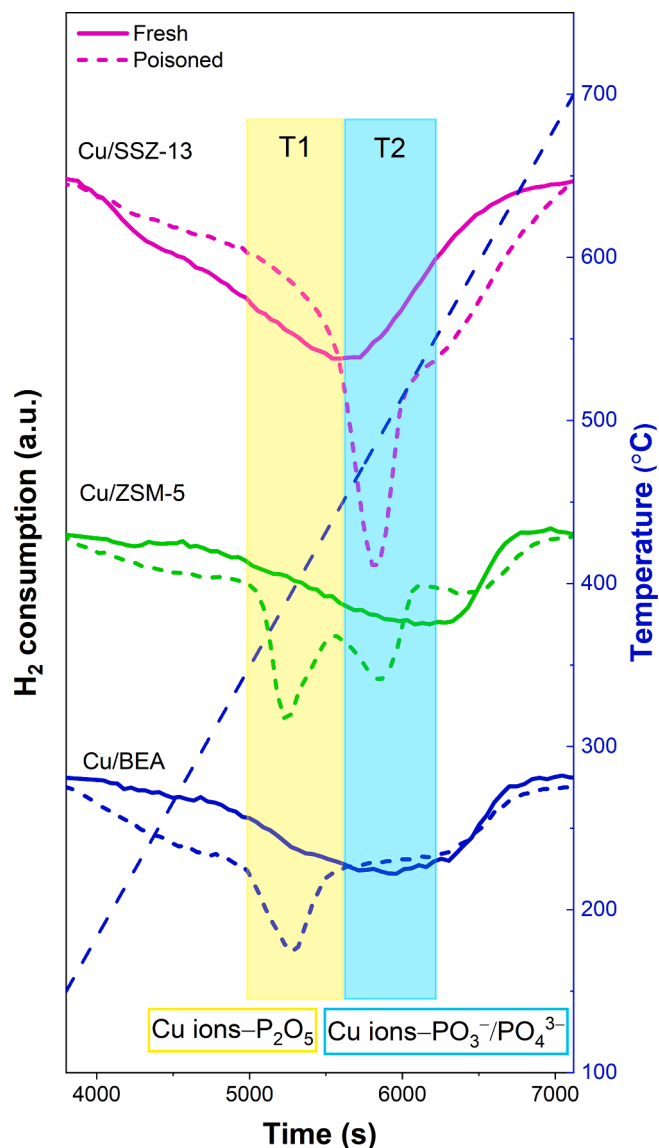
Fig. 5. H$_2$-TPR profiles of fresh and P-poisoned Cu/BEA, Cu/ZSM-5 and Cu/SSZ-13 samples.

mixture was used to investigate the redox capacity of Cu ions in conditions close to the real operating SCR environment. The samples were first pre-oxidized at 550 °C in 8 % O$_2$/Ar for 30 min and then cooled to 50 °C under the same gas flow. Subsequently, the O$_2$ was turned off, and 400 ppm NO/400 ppm NH$_3$ was fed into the gas phase at 50 °C, and maintained for 1 h. Finally, the temperature was ramped from 50 °C to 400 °C at 20 °C /min. The full profiles of the NO-NH$_3$-TPR results for all the fresh and P-poisoned samples are shown in Fig. S3, and the enlarged NO consumption parts are presented in Fig. 6a. As can be seen, the three types of Cu/zeolite revealed diverse reduction behaviors after phosphorus poisoning, which clearly illustrates that phosphorus had different effects on the redox capacity of the Cu ions in the three samples. Since no NO consumption was found for the P-poisoned H/SSZ-13 sample using the NO-TPR test (not shown), so we assume that phosphorus species were not reducible by NO. The subtracted curves (i.e., the NO-NH$_3$-TPR curve for fresh samples (solid line) minus that for poisoned samples (dashed line)) are presented in Fig. 6b.

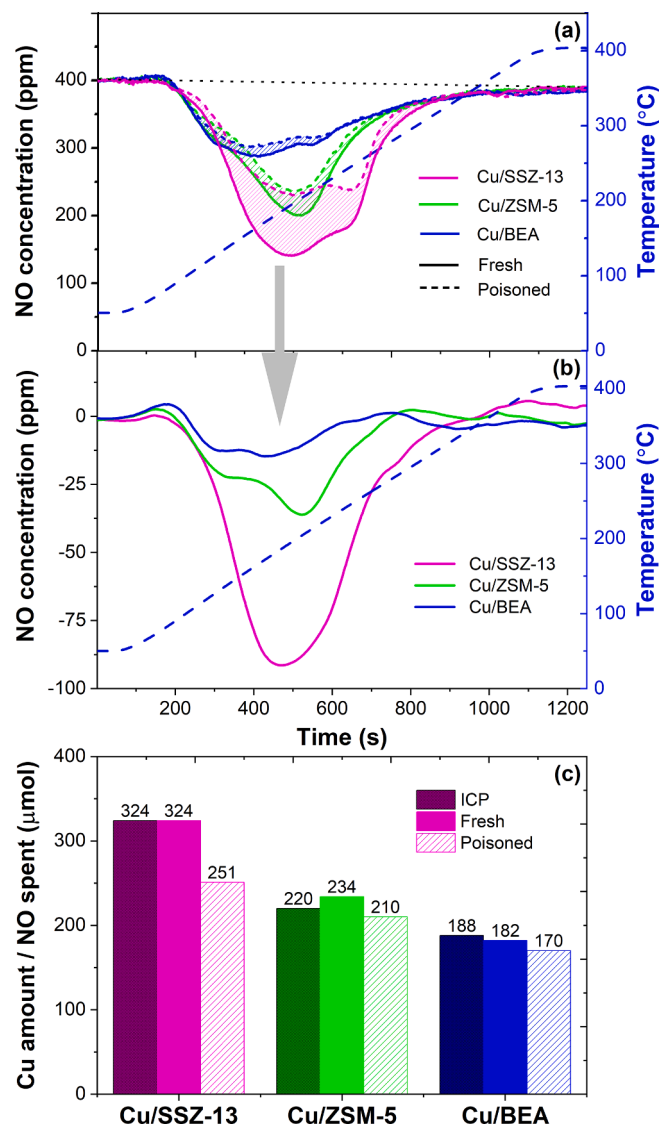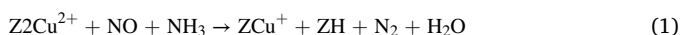According to the literature [44], the reactions for Cu ion (i.e., Z2Cu and ZCuOH) reduction are as follows:

$$Z2Cu^{2+} + NO + NH_3 \rightarrow ZCu^+ + ZH + N_2 + H_2O \tag{1}$$

Fig. 6. (a) NO-NH$_3$-TPR profiles for fresh (solid lines) and P-poisoned (dashed lines) Cu/BEA, Cu/ZSM-5 and Cu/SSZ-13 samples;(b) The curves subtracted from the NO-NH$_3$-TPR of Cu/BEA, Cu/ZSM-5 and Cu/SSZ-13 samples; (c)) Integrated NO consumption amount (μmol, normalized to 700 mg washcoat) for the fresh and P-poisoned Cu/BEA, Cu/ZSM-5 and Cu/SSZ-13 samples together with ICP results.

$$ZCu^{2+}OH + NO + NH_3 \rightarrow ZCu^+ + N_2 + 2H_2O \tag{2}$$

Reactions (1) and (2) indicate that the reduction of one copper ion, either Z2Cu or ZCuOH, requires the consumption of one NO and one NH$_3$ [43,44]. The NO consumption areas were therefore integrated, and the obtained results are shown in Fig. 6c. The Cu amount (μmol) calculated from ICP results is shown for comparison. These values were normalized to NO consumption from 700 mg washcoat. The amount of NO consumed by the fresh samples was the same as the amount of copper from the ICP results, which confirms the above reactions and also shows that the Cu species in the three samples were mainly in the form of Cu ions since CuO$_x$ clusters do not consume NO. The order in which Cu ions were affected is: Cu/SSZ-13 > Cu/ZSM-5 > Cu/BEA. This is consistent with the XPS, NH$_3$-TPD, and H$_2$-TPR results and also confirms that PO$_3^-$/PO$_4^{3-}$ possesses the most negative influence on the redox ability of Cu ions in real SCR conditions. Note that the decrease in the crystallinity of Cu/ZSM-5 was not reflected in a sharp decline in effective

Cu ions, where most Cu ions were still ion-exchanged to the framework. Combined with the data from NH$_3$-TPD experiments, it can be suggested that the minor destruction of the Cu/ZSM-5 structure was due to the phosphorus attacking the surface defects of the zeolite. In addition, the zeolite diffraction peaks (Fig. 1c) shifted to lower angles in the P-poisoned Cu/ZSM-5 sample than in its fresh counterpart, suggesting that the phosphorus caused local expansion and minor breakage of the structure. However, this low level of destruction does not seem to cause any large-scale loss of Brønsted acid sites and Cu active sites, but it does block the zeolite pores to a certain extent and leads to a decrease in specific surface area and pore volume.

Previous studies [21,37,45] have suggested that ZCuOH is easily affected by sulphur/phosphorus poisoning. Therefore, NO$_2$ adsorption/desorption experiments were conducted to quantitatively probe the extent to which ZCuOH is affected by phosphorus poisoning in different zeolites, as shown in Fig. 7a (adsorption region) and Fig. 7b (desorption region). Recent studies [44] have demonstrated that only ZCuOH can adsorb NO$_2$ in the form of nitrates; the equation is as follows:

$$2ZCu^{2+}OH^- + 3NO_2 \rightarrow 2ZCu^{2+}NO_3^- + NO + H_2O \qquad (3)$$
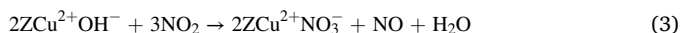
One ZCuOH site can form one nitrate species, which decomposes and desorbs one NO$_2$. Every-two nitrates produced release one NO. Therefore, the theoretical ratio of ZCuOH: NO$_2$ desorbed: NO released is 2: 2: 1. The integrated areas of released NO and desorbed NO$_2$ are shown in Table 2, and the NO/NO$_2$ ratios are further calculated and shown in the

Table 2

NO released amount, NO$_2$ desorbed amount, NO/NO$_2$ ratios, ZCuOH amount obtained from NO$_2$-TPD experiments, Cu$_{total}$ calculated from ICP, and the percentage of ZCuOH.

Sample	NO released (µmol)	NO$_2$ desorbed (µmol)	NO/NO$_2$ ratio	ZCuOH* (µmol) (NO$_2$-TPD)	Cu$_{total}$ (µmol) (ICP)	ZCuOH/Cu$_{total}$ (%)
Cu/SSZ-13_F	92	210	0.44	197	324	61
Cu/SSZ-13_P	64	149	0.43	138	304	44
Cu/ZSM-5_F	79	137	0.57	147	220	67
Cu/ZSM-5_P	68	120	0.56	128	209	61
Cu/BEA_F	74	144	0.52	146	188	77
Cu/BEA_P	72	130	0.55	137	188	73

* ZCuOH = [(NO released)*2 + (NO$_2$ desorbed)]/2.

table. All the amounts (µmol) were normalized based on 700 mg of washcoat. As expected, the obtained NO/NO$_2$ ratios for all the samples were ca 0.5 (0.4 ~ 0.6), which is consistent with Reaction (3).

The content of ZCuOH was obtained by averaging of the amount of released NO and desorbed NO$_2$ (ZCuOH = [(NO released)*2 + (NO$_2$
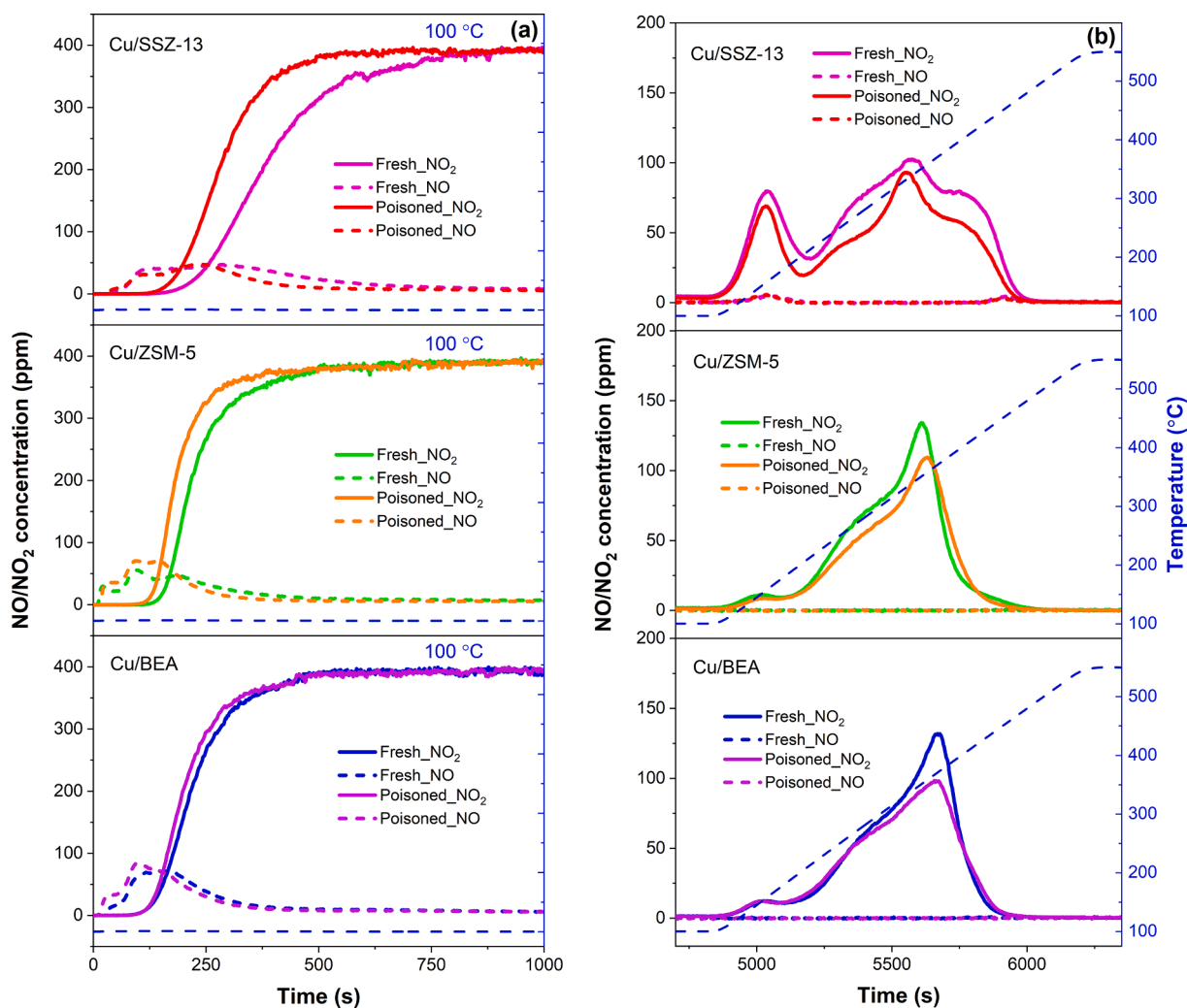

Fig. 7. NO$_2$-TPD profiles. (a) NO$_2$ adsorption region for fresh and P-poisoned Cu/BEA, Cu/ZSM-5 and Cu/SSZ-13 samples;(b) NO$_2$ desorption region for fresh and P-poisoned Cu/BEA, Cu/ZSM-5 and Cu/SSZ-13 samples.

desorbed)]/2), to minimize small experimental errors. The total amount of Cu in the samples calculated from ICP is also presented in Table 2. Consequently, the percentage of ZCuOH in the total Cu ions of the samples can be obtained. After phosphorus poisoning, approximately 28 %, 9 %, and 5 % (calculated using (ZCuOH$_{Fresh}$ − ZCuOH$_{Poisoned}$) / ZCuOH$_{Fresh}$) of ZCuOH in the Cu/SSZ-3, Cu/ZSM-5, and Cu/BEA samples, respectively, lost the capacity to adsorb NO$_2$. This is in line with the results from NH$_3$-TPD and NO-NH$_3$-TPR, which showed that Cu/SSZ-13 was the most affected of the samples.

Two types of Cu ions, Z2Cu and ZCuOH, were identified as present in the Cu/zeolites, and these sites behaved differently in their capacity to store NH$_3$; one Z2Cu site could adsorb four ammonia molecules, while one ZCuOH site could only adsorb three ammonia molecules [44,46]. The NH$_3$-TPD data presented in Fig. 3 and Fig. 4 can be used to calculate the loss in the capacity of Cu ions to store NH$_3$ after phosphorus poisoning. For instance, the decrease in the capacity of Cu ions in Cu/SSZ-13 to store NH$_3$ was (1261–982) × 69 % = 193 μmol. NO-NH$_3$-TPR results (Fig. 6) also gave information on Cu ions that lose redox ability in real SCR conditions after phosphorus poisoning, e.g., the amount of deactivated Cu ions in Cu/SSZ-13 was around (324–251) = 73 μmol. As mentioned above, one Z2Cu can store four ammonia molecules, and one ZCuOH can store three ammonia molecules. We found that multiplying this value by three approached the amount of the reduction in the NH$_3$ storage capacity of the Cu ions (219 μmol vs 193 μmol). This could suggest that the Cu ions that are poisoned and lose their redox ability are mostly ZCuOH.

To further support this suggestion, the amount of ZCuOH poisoned by phosphorus was obtained from NO$_2$-TPD profiles (Fig. 7 and Table 2). The poisoned ZCuOH in Cu/SSZ-13 was around (197–138) = 59 μmol. This value multiplied by three gives the loss of NH$_3$ storage capacity caused by ZCuOH poisoning as equal to 177 μmol. Considering the experimental errors, these three values, i.e., 193 μmol from NH$_3$-TPD, 219 μmol from NO-NH$_3$-TPR, and 177 μmol from NO$_2$-TPD, can be considered consistent. These findings suggest that ZCuOH in Cu/SSZ-13 had lost its redox functionality and ability to adsorb NH$_3$ due to phosphorus poisoning. The same calculations and comparisons were also applied to Cu/ZSM-5 and Cu/BEA. All the results are shown in Fig. 8. The above finding clearly applies to all three catalyst systems. A recent study by our group [21] has suggested that the poisoning of Z2Cu involves P$_2$O$_5$, but the interacted phosphorus species was PO$_3^-$/PO$_4^{3-}$ for

ZCuOH contamination. This finding can explain why BEA was less affected by phosphorus poisoning, mainly because phosphorus exists to large extent in the form of P$_2$O$_5$.

3.2. Catalytic tests

As shown in Fig. 9, NH$_3$ oxidation kinetics give some interesting differences for fresh and P-poisoned samples with different framework structures. A significant decrease in NH$_3$ conversions was found for the Cu/SSZ-13 sample after phosphorus poisoning [20,21]. Interestingly, the performance of the other two Cu/zeolites towards NH$_3$ oxidation increased after phosphorus poisoning, especially the Cu/ZSM-5 sample. For example, the NH$_3$ conversion of P-poisoned Cu/ZSM-5 increased from 56 % to 76 % at 550 °C compared to its fresh counterpart·NH$_3$ conversions at 550 °C for Cu/BEA after phosphorus poisoning changed from 31 % to 36 %. Both CuO$_x$ clusters and Cu ions (Z2Cu and ZCuOH) possess the ability for NH$_3$ oxidation [25]. Therefore, the increased/decreased catalytic activity for NH$_3$ oxidation could be closely related to the changes in CuO$_x$ clusters and/or Cu ions. Combined with the XPS, TPD, and TPR results, the dramatic decrease in the activity of the P-poisoned Cu/SSZ-13 sample could be caused by the poisoning of Cu ions by PO$_3^-$/PO$_4^{3-}$ species [21,22]. Considering some destruction of the zeolite framework of the P-poisoned Cu/ZSM-5, the increase in its catalytic activity towards NH$_3$ oxidation suggests that a small amount of Cu ions had detached from the framework to form CuO$_x$ clusters. As the CuO$_x$ clusters were very active for NH$_3$ oxidation at high temperature [17], and the decrease in Cu ions was minor, according to NH$_3$-TPD, NO-NH$_3$-TPR, and NO$_2$-TPD results for P-poisoned Cu/ZSM-5, the detached Cu ions were very limited.

It was interesting to observe the small increase in the activity of P-poisoned Cu/BEA, which showed no destruction, as seen in the XRD results. XPS results (Fig. 2) revealed that the dominant phosphorus species in P-poisoned Cu/BEA was P$_2$O$_5$, accounting for more than 80 %. The increase in activity in this context is not believed to be due to the formation of new CuO$_x$ species, which was supported by findings from an NH$_3$-SCR test shown later where the selectivity for high temperature remained good [25]. H$_2$-TPR profiles indicate that the presence of P$_2$O$_5$ shifted the reduction temperature of Cu ions to low temperatures in Cu/BEA. Therefore, we propose that P$_2$O$_5$ slightly enhanced the redox ability of Z2Cu in P-poisoned Cu/BEA, which results in a minor increase in NH$_3$ conversion.

Fig. 10a presents steady-state NO conversion as a function of time
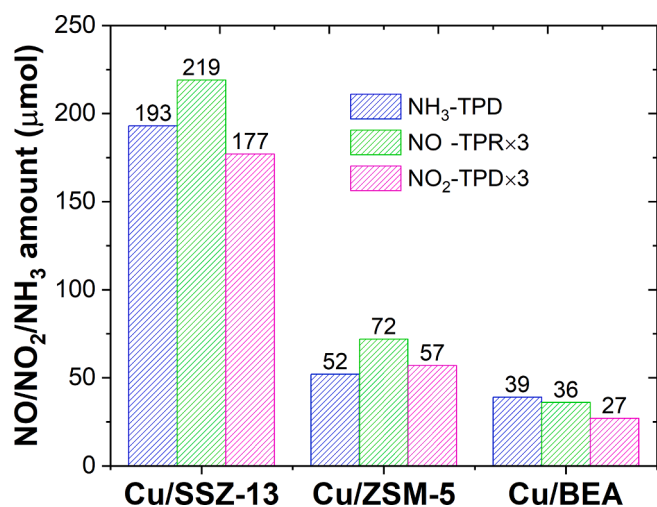
Fig. 8. A comparison of the loss of NH$_3$ storage capacity on Cu ions were for Cu/BEA, Cu/ZSM-5 and Cu/SSZ-13 samples determined based on (NH$_3$ desorption of Fresh-NH$_3$ desorption of Poisoned) * Cu ions percentage from XPS; the deactivated Cu ions from NO-NH$_3$-TPR × 3 ((NO spent of Fresh –NO spent of Poisoned)*3)); and the poisoned ZCuOH from NO$_2$-TPD × 3 ((NO$_2$ desorption of Fresh-NO$_2$ desorption of Poisoned)*3).

Fig. 9. The conversion of NH$_3$ oxidation as a function of temperature for fresh and P-poisoned Cu/BEA, Cu/ZSM-5 and Cu/SSZ-13 samples.

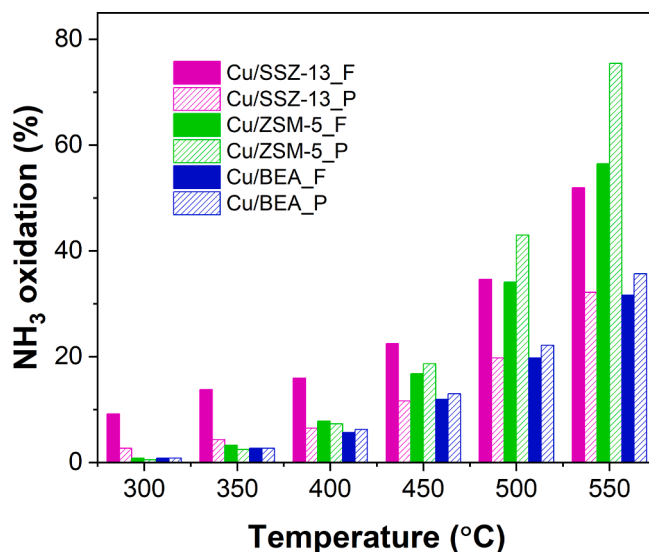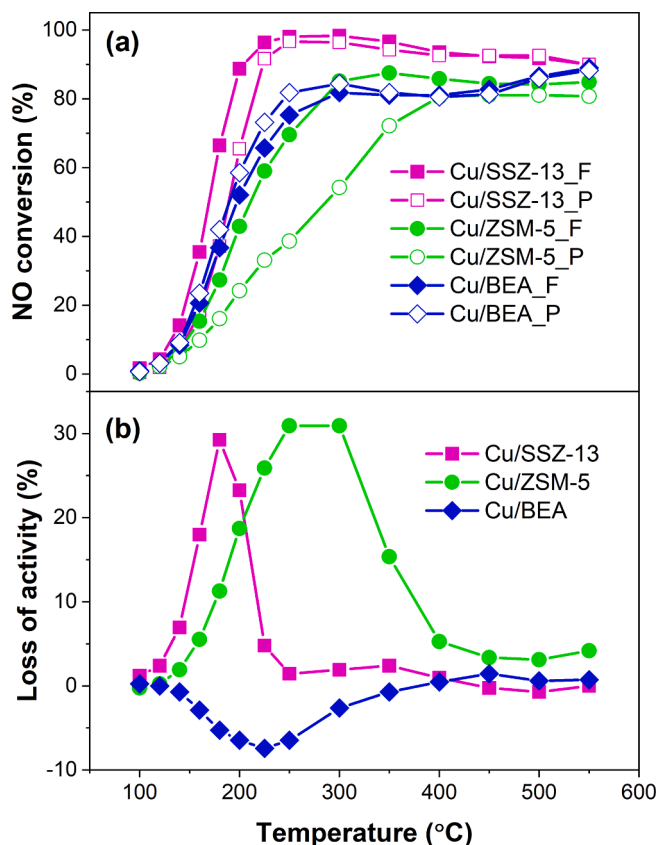**Fig. 10.** (a) NO conversion as a function of temperature during standard NH$_3$-SCR experiments for fresh and P-poisoned Cu/BEA, Cu/ZSM-5 and Cu/SSZ-13 samples; (b) The curves subtracted from the NO conversion of Cu/BEA, Cu/ZSM-5 and Cu/SSZ-13 samples.

from an NH$_3$-SCR experiment for fresh and P-poisoned Cu/BEA, Cu/ZSM-5 and Cu/SSZ-13 catalysts. Significant differences can be found in the NH$_3$-SCR performance of the three samples after phosphorus poisoning. To better understand the effects of phosphorus poisoning, the subtracted curves (i.e., the SCR curve for fresh samples minus that for poisoned samples, i.e., *Loss of activity (%) = C$_{fresh}$ − C$_{poisoned}$, C represents NO conversion*) are presented in Fig. 10**b**. The affected activities of the three samples all occurred in the low- and medium-temperature areas, around 100 ~ 300 °C for Cu/SSZ-13 and Cu/BEA, and around 100 ~ 400 °C for Cu/ZSM-5. The P-poisoned Cu/BEA, surprisingly, showed better NO conversion in the low-temperature region than its fresh counterpart. This is the complete opposite of findings for Cu/SSZ-13 and Cu/ZSM-5 samples, where negative effects were observed.

This phenomenon for Cu/BEA can be explained based on the above characterization results. Only ZCuOH was found to lose its ability to adsorb NH$_3$ and redox due to phosphorus poisoning, and as summarized in Fig. 8, Cu/BEA was the least affected sample. In addition, at low temperature P$_2$O$_5$ is suggested to enhance the redox ability of Z2Cu in P-poisoned Cu/BEA, which results in an increase in its activity in NH$_3$-SCR. The low-temperature deactivation of Cu/SSZ-13 can be explained by ZCuOH being significantly poisoned by PO$_3^-$/PO$_4^{3-}$. In addition, Guo et al. [47] have found using impedance spectroscopy that P also hinders the movement of the Cu species. Interestingly, the activity of Cu/ZSM-5 also showed a large decline in low-temperature conditions, and Cu ions and Brønsted acid sites did not show any significant decrease. Why did the active sites remain while the activity of the catalyst was seriously reduced? We can see that the activity in the high-temperature region (greater than400 °C) was not greatly affected. This is a reminder of the low-temperature reaction mechanism of NH$_3$-SCR. Due to the need to activate O$_2$, Gao et al. [35] and Paolucci et al. [34] have addressed the

evolution of (NH$_3$)$_2$Cu^{2+}−O$_2$ − Cu^{2+}(NH$_3$)$_2$ through mobile NH$_3$-solvated Cu ions, which are significantly more active for the dissociation of O$_2$ than a single Cu ion site. This suggests that two isolated Cu ions are required for efficient O$_2$ activation at low temperature. According to XRD and BET results, local expansion and cracking happened because the phosphorus attacked the surface defects of the zeolite, which can block the pore cages to a certain extent. We suggest that a possible reason for the decreased low temperature activity is that the P blockage might affect the free movement of ammonia-solvated Cu ions in low-temperature conditions, thereby reducing the probability of the formation of (NH$_3$)$_2$Cu^{2+}−O$_2$ − Cu^{2+}(NH$_3$)$_2$. The reaction mechanism in high-temperature conditions is completely different, where only one Cu ion is needed [34,35]. This can be one reason why the high-temperature activity was not affected. In addition, at high temperature the ammonia conversion is usually very high and limits the NOx conversion, by lowering the selectivity, and when there is high conversion it could be difficult to assess the deactivation.

The effect of phosphorus poisoning on the formation of N$_2$O in NH$_3$-SCR experiments was further investigated for fresh and P-poisoned samples, as shown in Fig. S4. It is well known that the N$_2$O formation of Cu/zeolite catalysts presents a low-temperature peak located at around 200 ~ 250 °C [48]. The formation of N$_2$O in high-temperature conditions (greater than350 °C) can be attributed to the un-selective NH$_3$-SCR [25]. Clearly, the amount of N$_2$O produced by fresh Cu/BEA was much greater than that produced by fresh Cu/SSZ-13 and fresh Cu/ZSM-5, both in low- and high- temperature conditions. This result is consistent with previous findings [30]. The amount of N$_2$O produced by Cu/BEA increased after phosphorus poisoning, while the amount produced by Cu/SSZ-13 and Cu/ZSM-5 decreased, in line with NH$_3$-SCR results.

4. Conclusions

Three catalysts with different framework structures with comparable Si/Al and Cu/Al ratios, i.e., Cu/SSZ-13, Cu/ZSM-5, and Cu/BEA, were synthesized, and a theoretical phosphorus poisoning level of P/Cu equal to 1 was employed using the IWI method with a (NH$_4$)$_2$HPO$_4$ solution. Fresh and P-poisoned samples were used to study the effect of phosphorus on catalysts with different framework structures for standard SCR reactions. Multiple techniques, consisting of XRD, BET, XPS, various TPR and TPD, were used to gain an in-depth understanding of the deactivation and promotion mechanisms of these three samples after the addition of phosphorus.

The structures of Cu/SSZ-13 and Cu/BEA remained largely intact after phosphorus poisoning, however, the Cu/ZSM-5 sample clearly showed a decrease in the crystallinity of the zeolite as a result of phosphorus poisoning. We suggest that the minor destruction of the Cu/ZSM-5 structure occurred because phosphorus attacked the surface defects of the zeolite, causing local expansion and cracking.

The choice of zeolite framework for Cu/zeolites clearly affects the species formed during phosphorus poisoning. P$_2$O$_5$ was dominant in Cu/BEA, while PO$_3^-$/PO$_4^{3-}$ was the main species in Cu/SSZ-13, and the results for Cu/ZSM-5 were in between. One possible reason for this could be that the large pore size of Cu/BEA (CHA (~3.8 Å), MFI (~5.5 Å), to BEA (~6.6 Å)) results in less steric hindrance for the large P$_2$O$_5$ species. P$_2$O$_5$ is suggested to enhance the redox ability of Z2Cu in P-poisoned Cu/BEA, which results in an increase in its activity in NH$_3$-SCR reactions in low-temperature conditions. ZCuOH sites were significantly poisoned by the PO$_3^-$/PO$_4^{3-}$ in Cu/SSZ-13, resulting in low-temperature deactivation. The activity of the Cu/ZSM-5 sample also showed a great decline in low-temperature conditions but was well maintained in high-temperature conditions. It is suggested that the blockage of the zeolite pore in Cu/ZSM-5, caused by local expansion and some cracking, affected the free movement of ammonia-solvated Cu ions in low-temperature conditions. We speculate that this result reduced the probability of the formation of (NH$_3$)$_2$Cu^{2+}−O$_2$ − Cu^{2+}(NH$_3$)$_2$, which is a key step for O$_2$ activation. The reaction mechanism in high-temperature conditions was completely

different (i.e., only one Cu ion was required), which explains why high-temperature activity was not affected.

Declaration of Competing Interest

The authors declare that they have no known competing financial interests or personal relationships that could have appeared to influence the work reported in this paper.

Data availability

Data will be made available on request.

Acknowledgements

Appendix A. Supplementary data

Supplementary data to this article can be found online at https://doi.org/10.1016/j.cej.2022.140040.

References

[1] L. Han, S. Cai, M. Gao, J.-Y. Hasegawa, P. Wang, J. Zhang, L. Shi, D. Zhang, Selective Catalytic Reduction of NO_x with NH_3 by Using Novel Catalysts: State of the Art and Future Prospects, Chem. Rev. 119 (2019) 10916–10976.

[2] A. Wang, L. Olsson, The impact of automotive catalysis on the United Nations sustainable development goals, Nat. Catal. 2 (2019) 566–570.

[3] J. Kim, S.J. Cho, D.H. Kim, Facile Synthesis of KFI-type Zeolite and Its Application to Selective Catalytic Reduction of NO_x with NH_3, ACS Catal. 7 (2017) 6070–6081.

[4] J.H. Wang, H.W. Zhao, G. Haller, Y.D. Li, Recent advances in the selective catalytic reduction of NO_x with NH_3 on Cu-Chabazite catalysts, Appl Catal B-Environ 202 (2017) 346–354.

[5] E. Borfecchia, P. Beato, S. Svelle, U. Olsbye, C. Lamberti, S. Bordiga, Cu-CHA–a model system for applied selective redox catalysis, Chem. Soc. Rev. 47 (2018) 8097–8133.

[6] A. Wang, Y. Chen, E.D. Walter, N.M. Washton, D. Mei, T. Varga, Y. Wang, J. Szanyi, Y. Wang, C.H.F. Peden, F. Gao, Unraveling the mysterious failure of Cu/SAPO-34 selective catalytic reduction catalysts, Nat. Commun. 10 (2019) 1137.

[7] N. Martin, P.N.R. Vennestrom, J.R. Thogersen, M. Moliner, A. Corma, Fe-Containing Zeolites for NH_3-SCR of NO_x: Effect of Structure Synthesis Procedure, and Chemical Composition on Catalytic Performance and Stability, Chem-Eur J 23 (2017) 13404–13414.

[8] L. Wang, W. Li, S.J. Schmieg, D. Weng, Role of Bronsted acidity in NH_3 selective catalytic reduction reaction on Cu/SAPO-34 catalysts, J. Catal. 324 (2015) 98–106.

[9] C. Paolucci, A.A. Parekh, I. Khurana, J.R. Di Iorio, H. Li, J.D.A. Caballero, A.J. Shih, T. Anggara, W.N. Delgass, J.T. Miller, F.H. Ribeiro, R. Gounder, W.F. Schneider, Catalysis in a Cage: Condition-Dependent Speciation and Dynamics of Exchanged Cu Cations in SSZ-13 Zeolites, J. Am. Chem. Soc. 138 (2016) 6028–6048.

[10] K. Liu, H. He, Y.B. Yu, Z.D. Yan, W.W. Yang, W.P. Shan, Quantitative study of the NH3-SCR pathway and the active site distribution over CeWO$_x$ at low temperatures, J. Catal. 369 (2019) 372–381.

[11] P.S. Hammershoi, P.N.R. Vennestrom, H. Falsig, A.D. Jensen, T.V.W. Janssens, Importance of the Cu oxidation state for the SO_2-poisoning of a Cu-SAPO-34 catalyst in the NH_3-SCR reaction, Appl Catal B-Environ 236 (2018) 377–383.

[12] Y.N. Zhang, Y. Peng, K.Z. Li, S. Liu, J.J. Chen, J.H. Li, F. Gao, C.H.F. Peden, Using Transient FTIR Spectroscopy to Probe Active Sites and Reaction Intermediates for Selective Catalytic Reduction of NO on Cu/SSZ-13 Catalysts, ACS Catal. 9 (2019) 6137–6145.

[13] E. Borfecchia, K.A. Lomachenko, F. Giordanino, H. Falsig, P. Beato, A.V. Soldatov, S. Bordiga, C. Lamberti, Revisiting the nature of Cu sites in the activated Cu-SSZ-13 catalyst for SCR reaction, Chem. Sci. 6 (2015) 548–563.

[14] S. Roy, M.S. Hegde, G. Madras, Catalysis for NO_x abatement, Appl Energ 86 (2009) 2283–2297.

[15] A. Beretta, N. Usberti, L. Lietti, P. Forzatti, M. Di Blasi, A. Morandi, C. La Marca, Modeling of the SCR reactor for coal-fired power plants: Impact of NH_3 inhibition on Hg^0 oxidation, Chem. Eng. J. 257 (2014) 170–183.

[16] M. Zhu, J.-K. Lai, U. Tumuluri, Z. Wu, I.E. Wachs, Nature of active sites and surface intermediates during SCR of NO with NH_3 by supported V_2O_5–WO_3/TiO_2 catalysts, J. Am. Chem. Soc. 139 (2017) 15624–15627.

[17] J. Song, Y.L. Wang, E.D. Walter, N.M. Washton, D.H. Mei, L. Kovarik, M. H. Engelhard, S. Prodinger, Y. Wang, C.H.F. Peden, F. Gao, Toward Rational Design of Cu/SSZ-13 Selective Catalytic Reduction Catalysts: Implications from Atomic-Level Understanding of Hydrothermal Stability, ACS Catal. 7 (2017) 8214–8227.

[18] Z. Chen, C. Fan, L. Pang, S.J. Ming, P. Liu, T. Li, The influence of phosphorus on the catalytic properties, durability, sulfur resistance and kinetics of Cu-SSZ-13 for NO_x reduction by NH_3-SCR, Appl Catal B-Environ 237 (2018) 116–127.

[19] M.L. Tarot, E.E. Iojoiu, V. Lauga, D. Duprez, X. Courtois, F. Can, Influence of Na, P and (Na plus P) poisoning on a model copper-ferrierite NH_3-SCR catalyst, Appl Catal B-Environ 250 (2019) 355–368.

[20] K. Xie, A. Wang, J. Woo, A. Kumar, K. Kamasamudram, L. Olsson, Deactivation of Cu-SSZ-13 SCR Catalysts by Vapor-Phase Phosphorus Exposure, Appl Catal B-Environ 256 (2019), 117815.

[21] A. Wang, K. Xie, D. Bernin, A. Kumar, K. Kamasamudram, L. Olsson, Deactivation mechanism of Cu active sites in Cu/SSZ-13 Phosphorus poisoning and the effect of hydrothermal aging, Appl Catal B-Environ, (2020) 118781.

[22] K.P. Xie, J. Woo, D. Bernin, A. Kumar, K. Kamasamudram, L. Olsson, Insights into hydrothermal aging of phosphorus-poisoned Cu-SSZ-13 for NH_3-SCR, Appl Catal B-Environ 241 (2019) 205–216.

[23] H.W. Zhao, Y.N. Zhao, M.K. Liu, X.H. Li, Y.H. Ma, X. Yong, H. Chen, Y.D. Li, Phosphorus modification to improve the hydrothermal stability of a Cu-SSZ-13 catalyst for selective reduction of NO_x with NH_3, Appl Catal B-Environ 252 (2019) 230–239.

[24] D.W. Fickel, R.F. Lobo, Copper Coordination in Cu-SSZ-13 and Cu-SSZ-16 Investigated by Variable-Temperature XRD, J. Phys. Chem. C 114 (2010) 1633–1640.

[25] A. Wang, P. Arora, D. Bernin, A. Kumar, K. Kamasamudram, L. Olsson, Investigation of the robust hydrothermal stability of Cu/LTA for NH_3-SCR reaction, Appl Catal B-Environ 246 (2019) 242–253.

[26] K.P. Xie, K. Leistner, K. Wijayanti, A. Kumar, K. Kamasamudram, L. Olsson, Influence of phosphorus on Cu-SSZ-13 for selective catalytic reduction of NO_x by ammonia, Catal. Today 297 (2017) 46–52.

[27] A. Wang, J. Wang, S. Sheti, S. Dahlin, J. Han, J. Woo, K. Xie, L. Pettersson, L. Olsson, A deactivation mechanism study of phosphorus-poisoned Diesel Oxidation Catalysts: Model and supplier catalysts, Catal. Sci. Technol. 10 (2020) 5602.

[28] K. Wijayanti, S. Andonova, A. Kumar, J.H. Li, K. Kamasamudram, N.W. Currier, A. Yezerets, L. Olsson, Impact of sulfur oxide on NH3-SCR over Cu-SAPO-34, Appl Catal B-Environ 166 (2015) 568–579.

[29] M. Tajbakhsh, H. Alinezhad, M. Nasrollahzadeh, T.A. Kamali, Preparation, characterization and application of nanosized CuO/HZSM-5 as an efficient and heterogeneous catalyst for the N-formylation of amines at room temperature, J Colloid Interf Sci 471 (2016) 37–47.

[30] J.H. Kwak, D. Tran, S.D. Burton, J. Szanyi, J.H. Lee, C.H.F. Peden, Effects of hydrothermal aging on NH_3-SCR reaction over Cu/zeolites, J. Catal. 287 (2012) 203–209.

[31] G. Bettermann, W. Krause, G. Riess, T. Hofmann, Phosphorus compounds, inorganic, Ullmann's Encyclopedia of Industrial, Chemistry (2000).

[32] J. Shi, Y. Wang, W. Yang, Y. Tang, Z. Xie, Recent advances of pore system construction in zeolite-catalyzed chemical industry processes, Chem. Soc. Rev. 44 (2015) 8877–8903.

[33] T.V. Vineesh, V. Yarmiayev, D. Zitoun, Tailoring the electrochemical hydrogen evolution activity of Cu_3P through oxophilic surface modification, Electrochem. Commun. 113 (2020) 106691.

[34] C. Paolucci, I. Khurana, A.A. Parekh, S.C. Li, A.J. Shih, H. Li, J.R. Di Iorio, J. D. Albarracin-Caballero, A. Yezerets, J.T. Miller, W.N. Delgass, F.H. Ribeiro, W. F. Schneider, R. Gounder, Dynamic multinuclear sites formed by mobilized copper ions in NO_x selective catalytic reduction, Science 357 (2017) 898–903.

[35] F. Gao, D.H. Mei, Y.L. Wang, J. Szanyi, C.H.F. Peden, Selective Catalytic Reduction over Cu/SSZ-13: Linking Homo- and Heterogeneous Catalysis, J. Am. Chem. Soc. 139 (2017) 4935–4942.

[36] D. Jo, G.T. Park, T. Ryu, S.B. Hong, Economical synthesis of high-silica LTA zeolites: A step forward in developing a new commercial NH_3-SCR catalyst, Appl Catal B-Environ 243 (2019) 212–219.

[37] A. Wang, L. Olsson, Insight into the SO_2 poisoning mechanism for NO_x removal by NH_3-SCR over Cu/LTA and Cu/SSZ-13, Chem. Eng. J. 395 (2020) 125048.

[38] S. Lai, D. Meng, W. Zhan, Y. Guo, Y. Guo, Z. Zhang, G. Lu, The promotional role of Ce in Cu/ZSM-5 and in situ surface reaction for selective catalytic reduction of NO_x with NH_3, RSC Adv. 5 (2015) 90235–90244.

[39] A. Marberger, A.W. Petrov, P. Steiger, M. Elsener, O. Kröcher, M. Nachtegaal, D. Ferri, Time-resolved copper speciation during selective catalytic reduction of NO on Cu-SSZ-13, Nat. Catal. 1 (2018) 221–227.

[40] A. Wang, K. Xie, D. Bernin, A. Kumar, K. Kamasamudram, L. Olsson, Deactivation mechanism of Cu active sites in Cu/SSZ-13 — Phosphorus poisoning and the effect of hydrothermal aging, Appl Catal B-Environ 269 (2020), 118781.

[41] T. Nanba, S. Masukawa, A. Ogata, J. Uchisawa, A. Obuchi, Active sites of Cu-ZSM-5 for the decomposition of acrylonitrile, Appl Catal B-Environ 61 (2005) 288–296.

[42] B. Lucheva, T. Tsonev, R. Petkov, Method for obtaining of copper-phosphorus alloys, J Univ Chem Technol Metall 40 (2005) 235–238.

[43] P.S. Hammershoi, C. Negri, G. Berlier, S. Bordiga, P. Beat, T.V.W. Janssens, Temperature-programmed reduction with NO as a characterization of active Cu in Cu-CHA catalysts for NH_3-SCR, Catal, Sci Technol 9 (2019) 2608–2619.

[44] R. Villamaina, S. Liu, I. Nova, E. Tronconi, M.P. Ruggeri, J. Collier, A. York, D. Thompsett, Speciation of Cu Cations in Cu-CHA Catalysts for NH$_3$-SCR: Effects of SiO$_2$/AlO$_3$ Ratio and Cu-Loading Investigated by Transient Response Methods, ACS Catal. (2019) 8916–8927.

[45] Y. Jangjou, Q. Do, Y.T. Gu, L.G. Lim, H. Sun, D. Wang, A. Kumar, J.H. Li, L. C. Grabow, W.S. Epling, Nature of Cu Active Centers in Cu-SSZ-13 and Their Responses to SO$_2$ Exposure, ACS Catal. 8 (2018) 1325–1337.

[46] C. Paolucci, A.A. Parekh, I. Khurana, J.R. Di Iorio, H. Li, J.D. Albarracin Caballero, A.J. Shih, T. Anggara, W.N. Delgass, J.T. Miller, F.H. Ribeiro, R. Gounder, W. F. Schneider, Catalysis in a Cage: Condition-Dependent Speciation and Dynamics of Exchanged Cu Cations in SSZ-13 Zeolites, J. Am. Chem. Soc. 138 (2016) 6028–6048.

[47] A.Q. Guo, K.P. Xie, H.R. Lei, V. Rizzotto, L.M. Chen, M.L. Fu, P.R. Chen, Y. Peng, D. Q. Ye, U. Simon, Inhibition Effect of Phosphorus Poisoning on the Dynamics and Redox of Cu Active Sites in a Cu-SSZ-13 NH$_3$-SCR Catalyst for NO$_x$ Reduction, Environ. Sci. Technol. 55 (2021) 12619–12629.

[48] A.Y. Wang, Y.L. Wang, E.D. Walter, N.M. Washton, Y.L. Guo, G.Z. Lu, C.H.F. Peden, F. Gao, NH$_3$-SCR on Cu, Fe and Cu plus Fe exchanged beta and SSZ-13 catalysts: Hydrothermal aging and propylene poisoning effects, Catal. Today 320 (2019) 91–99.